https://doi.org/10.5194/tc-2019-230
Preprint. Discussion started: 7 October 2019

The Cryosphere Discussions

Projecting Circum-Arctic Excess Ground Ice Melt with a sub-grid representation in the Community Land Model

Lei Cai[1], Hanna Lee[1], Sebastian Westermann[2], Kjetil Schanke Aas[2]

[1]NORCE Norwegian Research Centre, Bjerknes Centre for Climate Research, 5008, Bergen, Norway
[2]Department of Geosciences, University of Oslo, Oslo, 0315, Norway

Correspondence to: Lei Cai (leca@norceresearch.no)

Abstract We implement a sub-grid representation of excess ground ice within permafrost soils and its melting using the latest version of Community Land Model (CLM5). Based on the original CLM5 tiling hierarchy, we duplicate the natural vegetated landunit by building extra tiles for up to three different excess ice conditions in each grid point. Single-grid simulation cases initialize the same amount of excess ice in same soil layers, while prescribing different volumetric ice contents and sub-grid distributions. For the same total amount of excess ice initialized at the same soil layers, different sub-grid variability of excess ice leads to different excess ice melting rates on the grid level, as well as to different impacts to permafrost thermal properties and local hydrology. We prescribed a tiling scheme based on the dataset "Circum-Arctic Map of Permafrost and Ground-Ice Conditions" (Brown et al., 2002) within horizontal and vertical distributions of three different types of excess ice in the CLM grid to test applicability of sub-grid representation. Compared to the excess ice initialized homogeneously in each grid, the sub-grid scale excess ice and the tiling scheme amend the overly early timing of initial melting and the overly high melting rate of excess ice in warming climate. Initializing the excess ice depths according to local active layer thickness reduces underestimation of excess ice melt for the Arctic coastal regions. Further developments rely on additional global observational datasets on both the spatial and vertical distributions of excess ground ice, where our development of sub-grid representation demonstrated the potential for more realistically projecting excess ice melt in the circum-Arctic domain.

1. Introduction

Permafrost soils are often underlain by different types of ground ice that exceed the pore space (Brown et al. 1997; Zhang et al., 1999). The presence of excess ground ice can alter permafrost thermal regime and landscape structure. Widespread thawing of permafrost is expected in a warmer future climate and modeling studies suggest large-scale degradation of near-surface permafrost at the end of 21st century (Lawrence *et al.* 2008 & 2011). Melting ground ice due to active layer thickening releases water as the form of surface and/or subsurface runoff, causing surface subsidence and modifying local hydrological cycle (West and Plug, 2008; Gross et al., 2011; Kokelj et al., 2013; Westermann et al., 2016).

Permafrost soils store massive amounts of carbon, which could be released to the atmosphere in the form of greenhouse gases upon thawing (Walter et al., 2006; Zimov et al., 2006; Schuur et al., 2008), possibly making a positive feedback to future climate (Koven et al., 2011; Schaefer et al., 2011; Burke et al., 2013). The existence of excess ice and its distribution in permafrost can significantly affect the rate of permafrost thawing, and in turn,

https://doi.org/10.5194/tc-2019-230
Preprint. Discussion started: 7 October 2019

The Cryosphere Discussions
Open Access EGU

the rate of soil carbon release (Hugelius et al., 2014). Therefore, more accurate projections of global scale excess ice melt has become an important task in order to enhance our understanding of permafrost thawing and the corresponding climatic impacts (Schuur et al., 2015; Turetsky et al., 2019).

In regional or local scale land modeling, higher resolution enables a more detailed representation of permafrost and excess ice. Available since version 3.6, a mosaic approach in the WRF-Noah system has provided a platform for sub-grid heterogeneity of land surface (Li et al., 2013). The tiling capability has helped to implement sub-grid snow in the Noah land model, improving model's performance over the mountainous regions in Norway (Aas et al., 2017). A two-tile approach allowing lateral heat exchange between sub-grids verifies that maintaining the existence of thermokarst ponds requires the heat loss from water to the surrounding land (Langer et al., 2016). The similar tiling approach has been applied on projecting the landscape changes due to permafrost thaw over ice wedge polygons and peat plateaus (Aas et al., 2019; Nitzbon et al., 2019).

On a global scale, the land component of Earth System Models (ESMs) have some capabilities of representing permafrost physics. In the Community Land Model (CLM), for example, the representation of permafrost-associated processes has been continuously improved over generations. By including key thermal and hydrological processes of permafrost, the CLM version 4 (CLM4) has reasonably reproduced the global distribution of permafrost (Lawrence et al., 2008; Lawrence et al., 2012; Slater and Lawrence, 2013). Projections based on the CLM4 under its highest warming scenario (RCP8.5) have shown over 50% degradation of near-surface permafrost by 2100 (Lawrence et al., 2012). Moreover, the recently released CLM5 has more advanced numerical implementations on most biogeophysical and biogeochemical processes (Lawrence et al., 2019). A refined soil profile and the upgraded snow accumulation and densification scheme in the CLM5 could contribute to simulating more realistic permafrost thermal regimes, whereas upgrades on biogeochemistry improve the projection of the soil carbon release in response to permafrost thaw. In addition, an excess ice physics scheme implemented by Lee et al. (2014) based on the CLM4.5 (CLM4.5_EXICE) allowed for a first-order simulation of surface subsidence globally by modeling excess ice melt under the warming climate.

The stratigraphy (i.e. depth distribution) of excess ice implemented in the model leads to differences in thaw trajectories in a warming climate. In nature, excess ice forms in a highly localized manner due to multiple combined processes and can vary in formation. For instance, ice lenses formed from frost heaving differ substantially in morphology from ice wedges formed from the melting and refreezing of penetrating water. Field measurements illustrate that the depth distribution of ground ice can vary over multiple types of excess ice body in a horizontal distance of 10 meters (Fritz et al., 2011). For instance, ground-penetrating radar measurements in the Northwest Territories, Canada, have detected complex spatial patterns containing multiple types of excess ice in a scale of 50 meters horizontally and 10 meters vertically beneath the surface (Pascale et al., 2008). The horizontal grid spacing of ESMs, on the other hand, usually ranges from one to two degrees (~100-200km horizontal scale), which makes it challenging to represent localized excess ice. The gap in spatial scale between model and real-world raises concerns for reliability of excess ice modeling in ESMs. Aside from the homogenously-initialized excess ice in the grid cell, CLM4.5_EXICE initializes excess ice in the same soil depths globally (below 1m), regardless of the varying active layer thickness in circum-Arctic permafrost areas. These

https://doi.org/10.5194/tc-2019-230
Preprint. Discussion started: 7 October 2019

The Cryosphere Discussions

deficiencies from the previous excess ice parameterization in the ESM hamper global excess ice projection from achieving higher accuracy.

To narrow the gap between the high spatial variability of excess ice and the coarse grid spacing in the ESMs, we applied a sub-grid approach in representing excess ice in permafrost soils within the CLM5 to investigate how existence and melting of excess ice affects land surface physics under warming climate. We conducted idealized single-grid simulations to examine the robustness of model development. We furthermore conducted global simulations with multiple case scenarios of excess ice initialization, aiming to bring the modeling of excess ice melt and the corresponding impacts in the global scale towards a higher accuracy.

2. Methodology

2.1 Sub-grid excess ice in the CLM5

The CLM5 utilizes a three-level tiling hierarchy to represent sub-grid heterogeneity of landscapes, which are, from top to bottom, landunits, columns, and patches (Olsen et al., 2010). There is only one column (the natural soil column) that is under natural vegetated landunit, which represents soil including permafrost. In this study, we modify the CLM5 tiling hierarchy by duplicating the natural vegetated landunit, making extra landunits for prescribing up to three different excess ice conditions in permafrost (Figure 1). We denote the duplicated landunits as "natural vegetated with low content of excess ice" (hereafter low ice landunit), "natural vegetated with medium content of excess ice" (hereafter mid ice landunit), and "natural vegetated with high content of excess ice" (hereafter high ice landunit). The original natural vegetated landunit then turns into "natural vegetated with no excess ice" (hereafter no ice landunit). The idea of this categorization follows that in the "Circum-Arctic Map of Permafrost and Ground-Ice Conditions" (CAPS, 2nd version; Brown et al., 2002) by National Snow & Ice Data Center (NSIDC; Figure 2). The sub-grid initial conditions of excess ice is read in as part of the surface data, which includes the variables of volumetric excess ice contents, depths of the top and bottom soil layer of added excess ice, and the area weights of landunits.

We adopted the same excess ice physics from CLM4.5_EXICE (Lee et al., 2014), including thermodynamic and hydrological processes. The added excess ice is evenly distributed within each soil layer, which in turn increases soil layer thickness. Because ice density is a constant, the increase of soil layer thickness is linearly proportional to the volumetric ice content. The revised algorithm for thermal conductivity and heat capacity of soil involves the effects of added excess ice. The revised phase change energy equation allows excess ice to melt. The meltwater adds to soil liquid water in the same soil layer, and it can move to the above layer if the original layer is saturated. Such numerical implementation replicates how the melt excess ice eventually converts to runoff and discharges from the soil. As excess ice melts, soil layer thickness decreases, which corresponds to surface subsidence due to excess ice melt. In our model parameterization, excess ice only melts and does not reform since the applied excess ice physics does not allow to reproduce the different formation process.

Aside from sub-grid tiles for excess ice, we acknowledge that the version upgrade from CLM4.5 to CLM5 as the base model could help better implementation of excess ice physics developed by Lee et al. (2014). By default, CLM5 represents soil with a 25-layer profile, for which the top 20 hydrologically-active layers cover 8.5

https://doi.org/10.5194/tc-2019-230
Preprint. Discussion started: 7 October 2019

meters of soil. There are additional 10 soil layers and it is 4.7 meters deeper compared to the default hydrologically-active soil layer profile in CLM4.5, not to mention the substantially more complex biogeophysical processes (Lawrence et al., 2019). We, therefore, developed the sub-grid representation of excess ice within the framework of the latest version of CLM, ensuring a longer lifespan of our developed code and leaving more possibilities for broader applications and further developments.

Testing the sub-grid representation of excess ice are conducted by both single-grid and global simulations. All simulations are forced by the 3rd version of Global Soil Wetness Project forcing data (GSWP3; Kim et al., 2012), running in the Satellite Phenology (SP) mode. The International Land Atmosphere Model Benchmarking (ILAMB; Collier et al., 2018) project has indicated superior performance of GSWP3 data forcing the CLM5 in the SP-only mode (http://webext.cgd.ucar.edu/I20TR/_build_090817_CLM50SPONLY_CRUNCEP_GSWP3_WFDEI/index.html). We conducted a 100-year spin-up using the 1901-1920 climatology before conducting historical period simulations covering 1901-2005. The purpose of spin-up simulations is to stabilize the soil thermal properties with excess ice. The 100-year length for spin-up is sufficient, as the SP-only mode does not involve any biogeochemical processes such as soil carbon accumulation. The anomaly forcing under the RCP8.5 scenario on top of the 1982-2005 climatology forces simulations in the projected period. The single-grid simulations run until 2300, while the global simulations stop by 2100 due to the limited computational resource. For the same reason, single-grid simulations apply refined soil profile with 49 hydrologically-active layers covering 10 meters of soil, while global simulations apply the default soil profile (20 hydrologically-active layers, 8.5 meters of soil). In both cases, there are five hydrologically-inactive bedrock layers below the soil layers, reaching 50 meters in depth. The duplicated landunits prolong computation time by roughly 10% compared to the original CLM5. We are, therefore, confident that our model development is highly efficient in addressing the sub-grid excess ice and subsequent permafrost thaw.

2.2 Single-grid simulations

We design idealized single-grid simulation cases, aiming to examine the effects of incorporating excess ice at the sub-grid scale to soil physics, i.e. whether different sub-grid scale distributions of excess ice differ reasonably from each other during excess ice melt. The results of single-grid simulations help to verify if the sub-grid representation of excess ice shows more potential in modeling excess ice compared to its previous version, where excess ice is homogeneously distributed in the CLM grid cell (Lee et al., 2014). We perform single-grid simulations over two sites, which are at the North Slope of Alaska (NSA; 70° N, 156° W) and to the Northeast of the city of Yakutsk (Yakutsk; 63° N, 130° E), respectively. These two sites have similar annual mean temperature and precipitation, while the seasonal variability in temperature is smaller in NSA as its adjacency to the Arctic Ocean brings a maritime climate in summer (Bieniek et al., 2012).

Both chosen sites have 100% natural soil to avoid the interference by other landunit types from the source. For sensitivity cases, volumetric ice contents for the low, medium, and high ice landunits are incorporated as 5%, 15%, and 25%, respectively, to be consistent with the CAPS data. For each site, we set up three excess ice cases with the same (or very close) grid-scale excess ice content but with different spatial variability. For each site, we design three cases, having a 100% area weight of low excess ice content (5% in volume; NSA_LL and

https://doi.org/10.5194/tc-2019-230
Preprint. Discussion started: 7 October 2019

Yakutsk_LL), a 33% area weight of medium excess ice content (15% in volume; NSA_ML and Yakutsk_ML), and a 20% area weight of high excess ice content (25% in volume; NSA_HL and Yakutsk_HL), respectively (Figure 2). For all of the soil layers between 1-4 meters (in the original soil profile before ice is added), excess ice is incorporated homogeneously, correspondingly increasing the thickness in these soil layers. The initialization depth of excess ice keeps the same as in Lee et al. (2014). The area weights store in the surface data file after multiplying the permafrost extent ratio. Both sites in the simulations are located in the continuous permafrost zone, therefore, we allocated the permafrost extent to 100% according to the CAPS data (Figure 3). Note that the CAPS data also categories these two sites into the high ice content area. The excess ice initialization scenario (5% grid-scale ice content, 1-4 meters depth) is not even close to reality, but rather represent idealized cases which allow examining the robustness of the sub-grid excess ice representation. Without input of realistic excess ice stratigraphies, simulation results cannot be expected to represent excess ice melt rates and timing as observed in the field.

2.3 Global simulations

The five global simulation cases aim to illustrate how the sub-grid excess ice representation can help portray more realistic initial condition of excess ice. We expect that these initial cryostratigraphies can help constrain circum-arctic excess ice melt under warming climate (Table 1). The CAPS data used to prescribe the initial condition of excess ice has a spatial resolution of 12.5 km, which is much higher resolution than the 1-degree grid spacing of the CLM5 simulation cases. Each of the five global simulation cases employs its own initialization scenario to upscale the excess ice condition from the CAPS data into the CLM grid. Case 1 initializes excess ice in the same manner as Lee et al. (2014), where the mean CAPS grid excess ice content is prescribed within the CLM grid as a constant in permafrost soil layers between 1-4 meters. Case 2 initializes excess ice in a sub-grid manner involving three excess ice landunits. The level of volumetric ice content that can contain excess ice set for case 2 follow the CAPS data, which are 5%, 15%, and 25%. The area weight of each excess ice landunit is calculated as the number of CAPS grids that have the corresponding excess ice content level (low, mid, or high) divided by the total number of CAPS grids in each CLM grid. The initialization depth of excess ice in case 2 keeps the same as in case 1.

Case 3 and 4 also initialize excess ice in a sub-grid manner, but by applying a tiling scheme, which prescribes the sub-grid distribution of three different types of excess ice. The levels of volumetric ice content are set to 25%, 45%, and 70% for the excess ice landunits. The three excess ice landunits intend to represent three different types of excess ice conditions in permafrost regions. We refer to a similar categorization made by O'neill et al. (2019) for Northern Canada in this study. In our tiling representation, the low ice landunit aims to represent segregated ice, which is consisted of ice lenses and layers that usually grow by frost heaving. The high ice landunit aims to represent ice-wedge terrain, which is formed from infilling and refreezing of meltwater in permafrost (Lachenbruch, 1962). Years of repeated cracking, meltwater infilling, and refreezing makes the wedged ice to grow gradually. Some ice wedges can grow as deep as tens of meters e.g. the Yedoma type ice (Ulrich et al., 2014). The ice contents for low and high ice landunits in this study follow the excess ice representation as the previous study that applied a similar excess ice physics (Aas et al., 2019). The medium ice landunit aims to represent relict ice preserved in permafrost since the past cold climate. Due to their nature and origin, the relict

https://doi.org/10.5194/tc-2019-230
Preprint. Discussion started: 7 October 2019

ice bodies could vary massively in morphology, while they are typically located deeper in the soil than the segregated ice (Fritz et al., 2015).

The CAPS permafrost map categorizes global permafrost areas by its extent (continuous, discontinuous, sporadic, and isolated), ground ice content (high, medium, and low), and overburden (thick and thin), making total 20 different variety in permafrost characteristics (Figure 3). One of the main challenges in incorporating CAPS data into the sub-grid excess ice representation is to upscale the excess ice condition prescribed by each CAPS variety to three excess ice landunits for each CLM grid. We design a tiling scheme prescribing the assignment of landunits for each CAPS types based on previous observations and empirical estimates (Table 2). In these simulations, we assume that all CAPS excess ice varieties have the same fraction of the low ice landunit (segregated ice), and the CAPS varieties with a higher ice content are due to the existence of the mid and/or high ice landunits. The assumption is based on observations that have found segregated excess ice widely distributed in the permafrost (Miller, 1972; Calmel and Allard, 2008). Summing up the landunit fractions for all the CAPS data within the CLM grid obtains the grid-scale area weights that are stored in the surface data file. The tiling scheme guarantees the same grid-scale excess ice distribution as in the first two cases, while with different sub-grid scale heterogeneities.

Excess ice in case 3 is incorporated in the same soil layers (between 1 and 4 meters) as case 1 and 2. Note that cases 1-3 do not represent realistic excess ice melt projections, as cryostratigraphies differ substantially throughout the circum-Arctic permafrost extent, with excess ice layers situated at different depths. On the other hand, comparing excess ice melt in these three cases allows us to understand the effects of initializing the ground column with different total amounts of excess ice. Case 4, on the other hand, represents a more realistic scenario, with excess ice layers starting at a predefined depth below the simulated (and thus spatially variable) active layer. This case is based on the assumption that ground ice was accumulated until just below the active layer during the spin-up period. Firstly, soil temperature of the control case in the spin-up period determines the active layer thickness for each grid point. Then for the low ice landunits, we add excess ice at soil layers within 0.2 to 1.2 meters below the active layer. For the medium ice landunits, we add excess ice at the layers between 1.2-3.2 meters below the active layer. For the high ice landunit, we add excess ice at the layers between 0.2 meters below the active layer and the top layer of hydrologically active soil layer (8.5 meters) in CLM. The high ice landunit in this study represents Yedoma type ice, as the corresponding CAPS varieties (e.g. ChL, ChH, and DhL) in central and eastern Siberia, as well as in Alaska, coincide geographically with the observed Yedoma regions (Kanevskiy et al., 2011; Grosse et al., 2013). Note that although adding excess ice increases soil layer thickness, it barely affects the active layer thickness, as the soil thickness above excess ice remains the same. Figure 4 shows a schematic plot for the initialization scenario in case 4. More details on the tiling scheme are in the discussion section.

https://doi.org/10.5194/tc-2019-230
Preprint. Discussion started: 7 October 2019

3. Results

3.1 Single-grid simulations

Differences in soil temperature and moisture from excess ice cases to control cases in single-grid simulations quantitatively show the effects of excess ice and its melting. In the shallower layers (0-2 m), excess ice results in slightly higher soil temperature in January (winter) but lower soil temperature in July (summer) relative to control cases, reducing the magnitude of seasonal cycle in soil temperature (Figure 5). In deeper layers (>2 m), the soil temperature in excess ice cases remains higher compared to control cases for both in summer and winter. The above responses in permafrost temperature results from the increases of specific heat and thermal conductivity of soil layer after incorporating excess ice. As the climate warms and permafrost thaws, the meltwater discharges in the form of runoff, eventually bringing soil temperatures in excess ice cases closer to that in the control case. For soil moisture, volumetric water content in July is higher in excess ice cases than control and is just above the permafrost table (Figure 6). As the active layer substantially deepens in the projected period for both sites, soil water in excess ice cases increases abruptly around 2180 for NSA while around 2150 for Yakutsk, indicating the degradation of permafrost in control cases. When permafrost degrades in the control case, the excess soil water in control cases starts of run off in the form of subsurface drainage, flushing out soil water and making the soil drier. Meanwhile, this has not occurred in excess ice cases yet, making the soil wetter in excess ice cases than in control cases. These responses in permafrost temperature and moisture after permafrost degradation are consistent with the results in Lee et al. (2014), suggesting that the excess ice physics developed in CLM4.5_EXICE performs reasonably in the sub-grid manner in CLM5. Among the three excess ice cases, the "LL" case shows the strongest responses in both soil temperature and soil water content. On the other hand, the effects of excess ice in soil temperature and moisture are weaker in the "ML" and "HL" cases, where the same amount of excess ice is distributed more localized within a fraction of grid.

Both sites exhibit active layer depth of around 0.5 m by the end of the spinup and active layer thickness does not increase substantially during the historical period (Black lines in Figure 5 and 6). For this reason, excess ice is incorporated one meter below the surface. No excess ice, therefore, melts during either the spin-up or the historical period simulations. Excess ice starts to melt around the 2070s in NSA_LL, while the timing is delayed for about 25 years in the other two cases for the same site (NSA_ML and NSA_HL; Figure 7). It is because the higher content of excess ice covering a smaller area takes longer to absorb enough latent heat of fusion from the atmosphere before it can start melting. Excess ice in NSA completely melts away in the 2170s, and the exact timing of which varies slightly (< 5 years) between cases. In Yakutsk, excess ice starts to melt earlier, but with a slower rate compared to NSA. Similar to the NSA cases, Yakutsk_ML and Yakutsk_HL exhibit delays in the timing of excess ice melt compared to Yakutsk_LL. Excess ice in Yakutsk_LL completely melts in the 2170s, while the timings of excess ice melting in Yakutsk_ML and Yakutsk_HL is delayed for about 10 to 15 years, respectively (Figure 7).

Excess ice melting supplies extra water to subsurface water storage, increasing soil water and eventually converting to runoff. The increases in surface runoff correspond well in timing with excess ice melt (Figure 7). Earlier permafrost thaw timing in control cases causes earlier increase in subsurface runoff and decrease in surface runoff than in excess ice cases. On the other hand, when the active layer depth reaches below the deepest soil

https://doi.org/10.5194/tc-2019-230
Preprint. Discussion started: 7 October 2019

layer in excess ice cases, more soil water from melt ice leads to the higher subsurface runoff compared to that in control cases. Among the three excess ice cases, the "LL" cases consistently exhibit the strongest and earliest responses in both surface and subsurface runoff as excess ice melts, being consistent with their earlier start of excess ice melt.

3.2 Global simulations

For case 1 with homogeneously-initialized excess ice in the grid scale, excess ice melting in the continuous permafrost regions in the year 2000 is negligible, while most melt is found over the subarctic region (Figure 8). Substantial amounts of excess ice melt around the circum-Arctic in 2050 for case 1. The regions with pronounced excess ice melt include Siberia, west coast of Alaska, and northwestern Canada at this time. For case 2 with the sub-grid representation of excess ice, the general patterns in excess ice melt resemble that in case 1 in both the spatial distribution and the magnitude (difference < 30 kg/m^2). As the amount of ice content in case 2 are identical to the CAPS data (5%, 15%, and 25%), the initial condition of grid-mean excess ice in case 2 remains the same as in case 1 for most grid points. This explains the minor difference in the magnitude of excess ice melt between case 2 and 1. In Siberia where there is a relatively high spatial heterogeneity of excess ice in the CAPS data, there are more grid points with different magnitude of excess ice melt in the grid scale between case 1 and 2. Although the difference between case 1 and 2 is small, this confirms the robustness of sub-grid representation of excess ice in the global simulation that the excess ice with higher ice content causes the melt to start later. Meanwhile, the small difference between case 2 and 1 suggests that the change in soil physics associated with excess ice melting is minor when only spatial resolution is increased, even though the sub-grid excess ice represents a more realistic soil ice distribution. Excess ice in case 3 melts substantially later than case 1 and 2, suggesting a more pronounced effect of more realistically representing various types of excess ice in the sub-grid initialization. The largest difference in excess ice melt from case 3 to case 1 is exhibited in central and eastern Siberia, while this is much smaller in Northern Canada and Alaska.

Case 4 simulates a similar amount of excess ice melt for most grid points around the circum-Arctic by 2000 (Figure 9). Such consistency in the magnitude of excess ice melt is due to the excess ice initialization applied in this study that all grid points with permafrost are assigned a low excess ice landunit, in which excess ice is consistently prescribed 0.2 meters below the active layer. Such initialization leads to a relatively similar initial melting time of excess ice. In some Arctic coastal areas in Alaska and Siberia with shallow active layer, no excess ice melts by 2000 in cases 1 to 3, while the amount of excess ice melting in case 4 by 2000 is about 10-30 kg m^{-2}. This amount of excess ice melt converts to 5-15 cm surface subsidence on the sub-grid scale, assuming only the low ice landunit is suffered from melting for these coastal regions. The magnitude of surface subsidence is comparable to the ~10 cm surface subsidence observed in Barrow and West Dock in the early 21st century (Shiklomanov et al., 2013; Streleskiy et al., 2017). The magnitude of surface subsidence is also comparable to the 1-4 cm decade^{-1} surface subsidence rate on average over the North Slope of Alaska observed by satellite measurements since the 1990s (Liu et al., 2010).

Within two respective Arctic regions in Eurasia (60-190 E, 60-80 N) and North America (190-300 E, 60-80 N) that are the two major Arctic sub-regions with substantial excess ice melt (Figure 8 and 9), the time series of excess ice melt are compared between cases. Excess ice starts to melt in the 1940s for both regions (Figure 10).

https://doi.org/10.5194/tc-2019-230
Preprint. Discussion started: 7 October 2019

Excess ice in case 1 melts the fastest, and the differences in the rate of excess ice melt from case 2 to case 1 are substantially smaller than those from case 3 to case 1. More excess ice melts in case 4 than in case 3 in Eurasia until 2050, after which the melting rate slows down in case 4, resulting in less melt in total than in case 3 by 2100. Similar features also present in the time series accumulated extra ground heat flux that quantifies the extra energy absorbed by permafrost to melt excess ice. With similar melting rates are observed in two regions before 2000, the excess ice melt in Eurasia is accelerated afterwards, resulting in 20-60 kg m^{-2} more excess ice melt on average compared to North America by 2100. The excess ice melt in different cases varies more from one another in Eurasia than in North America, due to higher spatial heterogeneity of the initialized excess ice in Eurasia. Regions with a more complex spatial distribution of excess ice exhibits the advantage of sub-grid excess ice developed in the CLM framework.

4. Discussions

The developed sub-grid representation of excess ice has shown the potential to more accurately represent excess ice melt on a global scale within the CLM framework. In the following, we discuss the limitations and remaining challenges in the application of sub-grid excess ice framework, and how this sub-grid representation can potentially help on other CLM model development.

Single-grid simulations have demonstrated the potential applicability of sub-grid representation of excess ice, particularly in representing a more realistic excess ice melt physics than the grid-scale excess ice in the CLM. Observations in Arctic Alaska showed that the volume of each individual excess ice amount is much larger than that in the CAPS data (Kanevskiy et al., 2013), as the CAPS data intends to describe large-scale excess ice distributions. Applying the large-scale excess ice condition to the sub-grid excess ice tiles, therefore, makes little difference in modeling excess ice melt from grid-scale excess ice initialization. The global simulation case 2, which is with sub-grid excess ice while directly applying excess ice content levels in the CAPS data, therefore, shows similar magnitude and spatial distribution of excess ice melt as in case 1. On the other hand, the initialization in case 4 represents the more more advantageous usage of sub-grid excess ice in the CLM framework, in which independent landunits are responsible for the modelling of different types of excess ice.

Both single-grid and global test simulations in this study have shown that the way excess ice melts under warming climate is also sensitive to its initial located depth. For the low and high ice landunits corresponding to segregated ice and wedged ice, initializing excess ice to just below the active layer could lead to reasonable results (Aas et al., 2019). The active-layer-dependent excess ice initialization in this study helps case 4 to maintain the melting rate in the early 2000s that is comparable to observations. For the medium ice landunit corresponding to relict ice, however, the depths and volumetric content of excess ice can vary substantially. Although the high ice landunit aims to represent Yedoma type ice that expands to the deepest soil layer, we argue that the soil depths for high excess ice content does not significantly affect the projection of excess ice melt by the end of 21st century. Single-grid simulations show active layer thickness of 2-3 meters in NSA and Yakutsk by 2100, which still does not reach the deepest soil layer in the model (8.5 meters deep). The unmelted part of the wedged ice bodies insignificantly affects the overall rate of excess ice melt, even though the remaining ice can slightly change soil temperature and moisture of the surrounding permafrost.

https://doi.org/10.5194/tc-2019-230
Preprint. Discussion started: 7 October 2019

On top of the original CLM with no excess ice melt and surface subsidence, the model development in this study has proved its capability in better representing permafrost thawing processes in the ESM framework. The comparison between global simulation cases in this study has suggested that the excess ice melt and the corresponding impacts are largely dependent on the initial condition of excess ice. The tiling scheme used in case 4 provides a possible scenario linking sub-grid excess ice distribution (including volumetric ice contents and located depths) to the CAPS data, which is derived from a combination of scattered observational results and empirical estimates. Therefore, we do not expect the modeled excess ice melt in this study to be highly accurate compared to observations. On the other hand, four global simulation cases exhibit how the sub-grid representation of excess ice helps excess ice modeling towards a more realistic representation of excess ice and permafrost thaw within the ESM framework. We emphasize that in order to give a better projection, more observational data is required to further evaluate and validate the new model implementation of excess ice. Unfortunately, no such global datasets exist that contains the necessary information on volumetric ice contents and depths of ice for different types of ice. In the regional scale, Jorgenson et al. (2008) present a permafrost map of total ground ice volume for the upper 5 meters of permafrost based on both observations and estimates for Alaska. In addition, O'Neill et al. (2019) have also made permafrost maps for Northern Canada by paleographic modeling, mapping the abundances of three types of excess ice respectively. Further improvements rely on more observation campaigns and/or observationally constrained datasets of excess ice contents and conditions globally.

To obtain the area weights of excess ice landunits for the global simulation case 3 and 4, we sum up the area weights of excess ice landunits, which are assigned by the tiling scheme (Table 2), of all CAPS points located within each CLM grid. Such an approach is technically feasible although the summation ignores the relative geographic locations of all CAPS points in each CLM grid, as CLM is not capable of addressing horizontal heat exchange between tiles. However, high-resolution land surface modeling involving complex landscape features, such as thermokarst ponds, cannot be represented reasonably if horizontal heat fluxes are ignored (Langer et al., 2016). Further developments on sub-grid scale horizontal heat exchanges in CLM will encounter the challenge in prescribing the relative geographic location of all sub-grid tiles in each CLM grid. One possible solution could be to prescribe sub-grid landscape feature in the surface dataset, such as the polygonal tundra and peat plateau in permafrost regions represented as in Aas et al. (2019). With such implementation, further developments could allow CLM "switching on" horizontal heat exchange between the geographically adjacent tiles. These ideas for future development much relies on the availability of observational data in permafrost stratigraphy. Therefore, we emphasize tight collaboration between observations and modeling.

5. Conclusion

This study develops a sub-grid representation of excess ice in the CLM5 and examines the impacts of the existence and melting of excess ice in the sub-grid scale under warming climate. Extra landunits duplicated from the natural vegetated landunit make the CLM sub-grid hierarchy possible to prescribe up to three different excess ice conditions in each grid point with permafrost.

This study, for the first time, brings the ESM-based excess ice modeling to the sub-grid scale globally, projecting excess ice melt under warming climate based on state-of-the-art knowledge on excess ice conditions.

The approach of duplicating tiles at landunit level instead of column level allows more freedom for further developments in this direction. Furthermore, the new CLM tiling hierarchy has much more potential than representing more accurate excess ice physics as examined in this study. Further applications on top of the sub-grid representation include, but are not limited to, the involvement of biogeochemistry (CLM5BGC) and snow redistribution due to the surface subsidence in the sub-grid scale. Combining the dynamic micro-topography developed by Ekici et al. (2019) with sub-grid scale excess ice representation may help better represent global projections of surface inundation under permafrost thaw. Further advancing the excess ice modeling relies on additional observational studies/datasets of the excess ground ice conditions on a global scale. The model development in our study therefore builds the foundation for further advances focusing on excess ice modeling and/or other processes in the CLM framework that could benefit from involving the sub-grid representation.

Code/Data Availability

The original Community Land Model is available at https://github.com/ESCOMP/ctsm. The source code of model development in this study is available from the corresponding author upon request.

Author contributions

L.C conducted model development work and wrote the initial draft with additional contributions with all authors. H.L, S.W and K.S.A provided ideas and help during the process of model development. H.L provided the code of excess ice physics in the earlier version of CLM. L.C prepared all figures.

Acknowledgments

This study is funded by the Research Council of Norway KLIMAFORSK program (PERMANOR; RCN#255331). We thank Sarah Chadburn for helpful comments and suggestions in preparing this manuscript.

Reference

Aas, K. S., Gisnås, K., Westermann, S., and Berntsen, T. K.: A Tiling Approach to Represent Subgrid Snow Variability in Coupled Land Surface–Atmosphere Models, Journal of Hydrometeorology, 18, 49-63, 10.1175/jhm-d-16-0026.1, 2017.

Aas, K. S., Martin, L., Nitzbon, J., Langer, M., Boike, J., Lee, H., Berntsen, T. K., and Westermann, S.: Thaw processes in ice-rich permafrost landscapes represented with laterally coupled tiles in a land surface model, The Cryosphere, 13, 591-609, 10.5194/tc-13-591-2019, 2019.

Bieniek, P. A., Bhatt, U. S., Thoman, R. L., Angeloff, H., Partain, J., Papineau, J., Fritsch, F., Holloway, E., Walsh, J. E., Daly, C., Shulski, M., Hufford, G., Hill, D. F., Calos, S., and Gens, R.: Climate Divisions for Alaska Based on Objective Methods, Journal of Applied Meteorology and Climatology, 51, 1276-1289, 10.1175/jamc-d-11-0168.1, 2012.

Brown, J., Ferrians Jr, O., Heginbottom, J., and Melnikov, E.: Circum-Arctic map of permafrost and ground-ice conditions, US Geological Survey Reston, VA, 1997.

https://doi.org/10.5194/tc-2019-230
Preprint. Discussion started: 7 October 2019

Burke, E. J., Dankers, R., Jones, C. D., and Wiltshire, A. J.: A retrospective analysis of pan Arctic permafrost using the JULES land surface model, Climate Dynamics, 41, 1025-1038, 10.1007/s00382-012-1648-x, 2013.

Calmels, F., and Allard, M.: Segregated ice structures in various heaved permafrost landforms through CT Scan, Earth Surface Processes and Landforms, 33, 209-225, 10.1002/esp.1538, 2008.

Ekici, A., Lee, H., Lawrence, D. M., Swenson, S. C., and Prigent, C.: Ground subsidence effects on simulating dynamic high latitude surface inundation under permafrost thaw using CLM5, Geosci. Model Dev. Discuss., https://doi.org/10.5194/gmd-2019-4, in review, 2019.

Collier, N., Hoffman, F. M., Lawrence, D. M., Keppel-Aleks, G., Koven, C. D., Riley, W. J., Mu, M., and Randerson, J. T.: The International Land Model Benchmarking (ILAMB) system: design, theory, and implementation, Journal of Advances in Modeling Earth Systems, 10, 2731-2754, 2018.

Grosse, G., Romanovsky, V., Jorgenson, T., Anthony, K. W., Brown, J., and Overduin, P. P.: Vulnerability and feedbacks of permafrost to climate change, Eos, Transactions American Geophysical Union, 92, 73-74, 2011.

Grosse, G., Robinson, J. E., Bryant, R., Taylor, M. D., Harper, W., DeMasi, A., Kyker-Snowman, E., Veremeeva, A., Schirrmeister, L., and Harden, J.: Distribution of late Pleistocene ice-rich syngenetic permafrost of the Yedoma Suite in east and central Siberia, Russia, US Geological Survey Open File Report, 2013, 1-37, 2013.

Hugelius, G., Strauss, J., Zubrzycki, S., Harden, J. W., Schuur, E. A. G., Ping, C. L., Schirrmeister, L., Grosse, G., Michaelson, G. J., Koven, C. D., O'Donnell, J. A., Elberling, B., Mishra, U., Camill, P., Yu, Z., Palmtag, J., and Kuhry, P.: Estimated stocks of circumpolar permafrost carbon with quantified uncertainty ranges and identified data gaps, Biogeosciences, 11, 6573-6593, 10.5194/bg-11-6573-2014, 2014.

Kanevskiy, M., Shur, Y., Fortier, D., Jorgenson, M. T., and Stephani, E.: Cryostratigraphy of late Pleistocene syngenetic permafrost (yedoma) in northern Alaska, Itkillik River exposure, Quaternary Research, 75, 584-596, 10.1016/j.yqres.2010.12.003, 2011.

Kim, H., Yoshimura, K., Chang, E., Famiglietti, J., and Oki, T.: Century long observation constrained global dynamic downscaling and hydrologic implication, AGU Fall Meeting Abstracts, 2012.

Kokelj, S. V., Lacelle, D., Lantz, T. C., Tunnicliffe, J., Malone, L., Clark, I. D., and Chin, K. S.: Thawing of massive ground ice in mega slumps drives increases in stream sediment and solute flux across a range of watershed scales, Journal of Geophysical Research: Earth Surface, 118, 681-692, 10.1002/jgrf.20063, 2013.

Koven, C. D., Ringeval, B., Friedlingstein, P., Ciais, P., Cadule, P., Khvorostyanov, D., Krinner, G., and Tarnocai, C.: Permafrost carbon-climate feedbacks accelerate global warming, Proceedings of the National Academy of Sciences, 108, 14769-14774, 2011.

Lachenbruch, A. H.: Mechanics of thermal contraction cracks and ice-wedge polygons in permafrost, Geological Society of America, 1962.

Langer, M., Westermann, S., Boike, J., Kirillin, G., Grosse, G., Peng, S., and Krinner, G.: Rapid degradation of permafrost underneath waterbodies in tundra landscapes—toward a representation of thermokarst in land surface models, Journal of Geophysical Research: Earth Surface, 121, 2446-2470, 2016.

Lawrence, D. M., Slater, A. G., Romanovsky, V. E., and Nicolsky, D. J.: Sensitivity of a model projection of near-surface permafrost degradation to soil column depth and representation of soil organic matter, Journal of Geophysical Research: Earth Surface, 113, 10.1029/2007JF000883, 2008.

Lawrence, D. M., Oleson, K. W., Flanner, M. G., Thornton, P. E., Swenson, S. C., Lawrence, P. J., Zeng, X., Yang, Z. L., Levis, S., and Sakaguchi, K.: Parameterization improvements and functional and structural advances in version 4 of the Community Land Model, Journal of Advances in Modeling Earth Systems, 3, 2011.

Lawrence, D. M., Koven, C. D., Swenson, S. C., Riley, W. J., and Slater, A. G.: Permafrost thaw and resulting soil moisture changes regulate projected high-latitude CO2and CH4emissions, Environmental Research Letters, 10, 094011, 10.1088/1748-9326/10/9/094011, 2015.

Lee, H., Swenson, S. C., Slater, A. G., and Lawrence, D. M.: Effects of excess ground ice on projections of permafrost in a warming climate, Environmental Research Letters, 9, 124006, 2014.

Li, D., Bou-Zeid, E., Barlage, M., Chen, F., and Smith, J. A.: Development and evaluation of a mosaic approach in the WRF-Noah framework, Journal of Geophysical Research: Atmospheres, 118, 11,918-911,935, doi:10.1002/2013JD020657, 2013.

Liljedahl, A. K., Boike, J., Daanen, R. P., Fedorov, A. N., Frost, G. V., Grosse, G., Hinzman, L. D., Iijma, Y., Jorgenson, J. C., and Matveyeva, N.: Pan-Arctic ice-wedge degradation in warming permafrost and its influence on tundra hydrology, Nature Geoscience, 2016.

Liu, L., Zhang, T., and Wahr, J.: InSAR measurements of surface deformation over permafrost on the North Slope of Alaska, Journal of Geophysical Research: Earth Surface, 115, 10.1029/2009jf001547, 2010.

Mackay, J. R.: Offshore permafrost and ground ice, southern Beaufort Sea, Canada, Canadian Journal of Earth Sciences, 9, 1550-1561, 1972.

Miller, R.: Freezing and heaving of saturated and unsaturated soils, Highway Research Record, 393, 1-11, 1972.

Nitzbon, J., Langer, M., Westermann, S., Martin, L., Aas, K. S., and Boike, J.: Pathways of ice-wedge degradation in polygonal tundra under different hydrological conditions, The Cryosphere, 13, 1089-1123, 10.5194/tc-13-1089-2019, 2019.

O'Neill, H. B., Wolfe, S. A., and Duchesne, C.: New ground ice maps for Canada using a paleogeographic modelling approach, The Cryosphere, 13, 753-773, 10.5194/tc-13-753-2019, 2019.

Schuur, E. A., Bockheim, J., Canadell, J. G., Euskirchen, E., Field, C. B., Goryachkin, S. V., Hagemann, S., Kuhry, P., Lafleur, P. M., and Lee, H.: Vulnerability of permafrost carbon to climate change: Implications for the global carbon cycle, BioScience, 58, 701-714, 2008.

Schuur, E. A. G., McGuire, A. D., Schädel, C., Grosse, G., Harden, J. W., Hayes, D. J., Hugelius, G., Koven, C. D., Kuhry, P., Lawrence, D. M., Natali, S. M., Olefeldt, D., Romanovsky, V. E., Schaefer, K., Turetsky, M. R., Treat, C. C., and Vonk, J. E.: Climate change and the permafrost carbon feedback, Nature, 520, 171, 10.1038/nature14338, 2015.

Shiklomanov, N. I., Streletskiy, D. A., Little, J. D., and Nelson, F. E.: Isotropic thaw subsidence in undisturbed permafrost landscapes, Geophysical Research Letters, 40, 6356-6361, 10.1002/2013gl058295, 2013.

Streletskiy, D. A., Shiklomanov, N. I., Little, J. D., Nelson, F. E., Brown, J., Nyland, K. E., and Klene, A. E.: Thaw Subsidence in Undisturbed Tundra Landscapes, Barrow, Alaska, 1962–2015, Permafrost and Periglacial Processes, 28, 566-572, 10.1002/ppp.1918, 2017.

Turetsky, M. R., Abbott, B. W., Jones, M. C., Anthony, K. W., Olefeldt, D., Schuur, E. A., Koven, C., McGuire, A. D., Grosse, G., and Kuhry, P.: Permafrost collapse is accelerating carbon release, in, Nature Publishing Group, 2019.

Ulrich, M., Grosse, G., Strauss, J., and Schirrmeister, L.: Quantifying wedge-ice volumes in Yedoma and thermokarst basin deposits, Permafrost and Periglacial Processes, 25, 151-161, 2014.

West, J. J., and Plug, L. J.: Time-dependent morphology of thaw lakes and taliks in deep and shallow ground ice, Journal of Geophysical Research: Earth Surface, 113, 10.1029/2006jf000696, 2008.

Westermann, S., Langer, M., Boike, J., Heikenfeld, M., Peter, M., Etzelmüller, B., and Krinner, G.: Simulating the thermal regime and thaw processes of ice-rich permafrost ground with the land-surface model CryoGrid 3, Geosci. Model Dev., 9, 523-546, 10.5194/gmd-9-523-2016, 2016.

Zhang, T., Barry, R. G., Knowles, K., Heginbottom, J. A., and Brown, J.: Statistics and characteristics of permafrost and ground-ice distribution in the Northern Hemisphere, Polar Geography, 23, 132-154, 10.1080/10889379909377670, 1999.

Zhang, T., Heginbottom, J. A., Barry, R. G., and Brown, J.: Further statistics on the distribution of permafrost and ground ice in the Northern Hemisphere, Polar Geography, 24, 126-131, 10.1080/10889370009377692, 2000.

Zimov, S. A., Schuur, E. A., and Chapin, F. S.: Permafrost and the global carbon budget, Science, 312, 1612-1613, 2006.

https://doi.org/10.5194/tc-2019-230
Preprint. Discussion started: 7 October 2019

Table 1: The list of global test cases established in this study and how excess ice is initialized.

Case No.	Excess ice initialzation	Excess ice content (volume percentage)			Excess ice Initialization depth (m)		
		Low ice landunit	Medium ice landunit	High ice landunit	Low ice landunit	Medium ice landunit	High ice landunit
control	No excess ice	N/A					
1	Homogenously distrbuted excess ice	Only one excess ice landunit in each grid			1-4 m		
2	Excess ice landunits with CAPS ice content	5%	15%	25%			
3	Excess ice landunits with the tiling scheme	25%	45%	70%			
4	Excess ice landunits with the tiling scheme in varied depth				ALD+0.2-ALD+1.2 m	ALD+1.2-ALD+3.2 m	ALD+0.2-8.5 m

*ALD = 1900s active layer depth

https://doi.org/10.5194/tc-2019-230
Preprint. Discussion started: 7 October 2019

The Cryosphere
Discussions
Open Access
EGU

Table 2: The tiling scheme prescribing area weights of landuntis for each CAPS variety.

Overall Ground ice content for each CAPS point	Tiling scheme (area weights for each excess ice category)	Eligible CAPS types
5%	20% Low	ClL; DlL; SiL; IlL; ClH; DlH; SiH; IlH
15%	20% Low; 22% Medium	CmL; DmL; SmL; ImL; DhH; ShH; IhH
15%	20% Low; 14% High	ChH
25%	20% Low; 22% Medium; 14% High	DhL; ShL; IhL
25%	20% Low; 28% High	ChL

505

https://doi.org/10.5194/tc-2019-230
Preprint. Discussion started: 7 October 2019

The Cryosphere
Discussions
Open Access

510

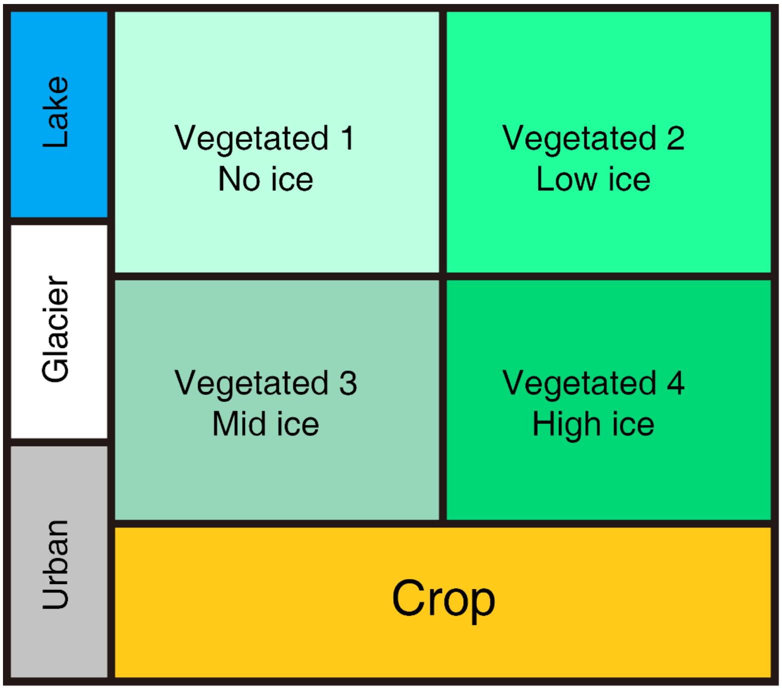

Figure 1: Modification of the CLM5 tiling hierarchy on the landunit level containing four natural vegetated landunits for different excess ice conditions.

https://doi.org/10.5194/tc-2019-230
Preprint. Discussion started: 7 October 2019

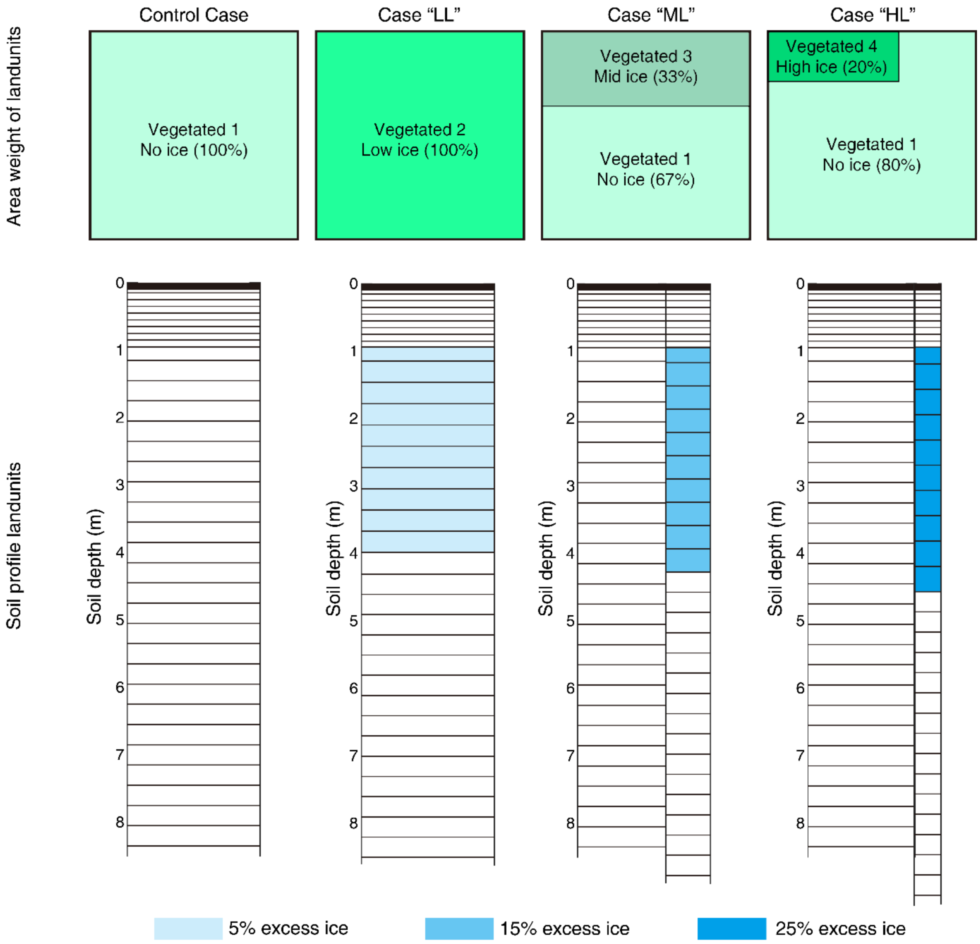

515 **Figure 2: The schematic figure for the area weights (the percentage between parentheses) and soil profiles within the landunits in the four single-grid simulations. Besides the control case, three other cases are with the same amount of excess ice within the single grid. “LL”, “ML”, and “HL” are abbreviations for “Low ice Landunit”, “Mid ice Landunit”, and “High ice Landunit”, representing the applied excess ice landunit in each case.**

https://doi.org/10.5194/tc-2019-230
Preprint. Discussion started: 7 October 2019

The Cryosphere
Discussions
Open Access

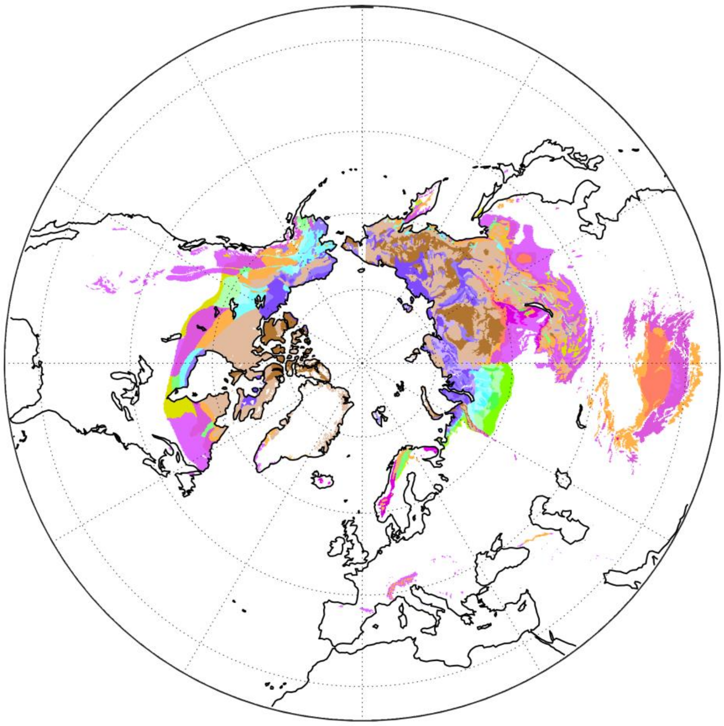

Permafrost Extent	Ground Ice Content (percent by volume)				
	Lowlands, highlands, and intra-and intermontane depressions			Mountains, highlands, ridges, and plateaus	
	25%	15%	5%	15%	5%
Continous (100%)	ChL	CmL	ClL	ChH	ClH
Discontinous (70%)	DhL	DmL	DlL	DhH	DlH
Sporadic (30%)	ShL	SmL	SlL	ShH	SlH
Isolated (5%)	IhL	ImL	IlL	IhH	IlH

*Letter code naming: the first letter is for the permafrost extent, the second is for the ground ice content, and the third for the topography.

Figure 3: Spatial distribution of excess ground ice globally in Brown et al. (2002). Compared to the original data, permafrost extents and ground ice contents are converted to definite numbers (percentages) for model computation.

https://doi.org/10.5194/tc-2019-230
Preprint. Discussion started: 7 October 2019

The Cryosphere
Discussions
Open Access

530
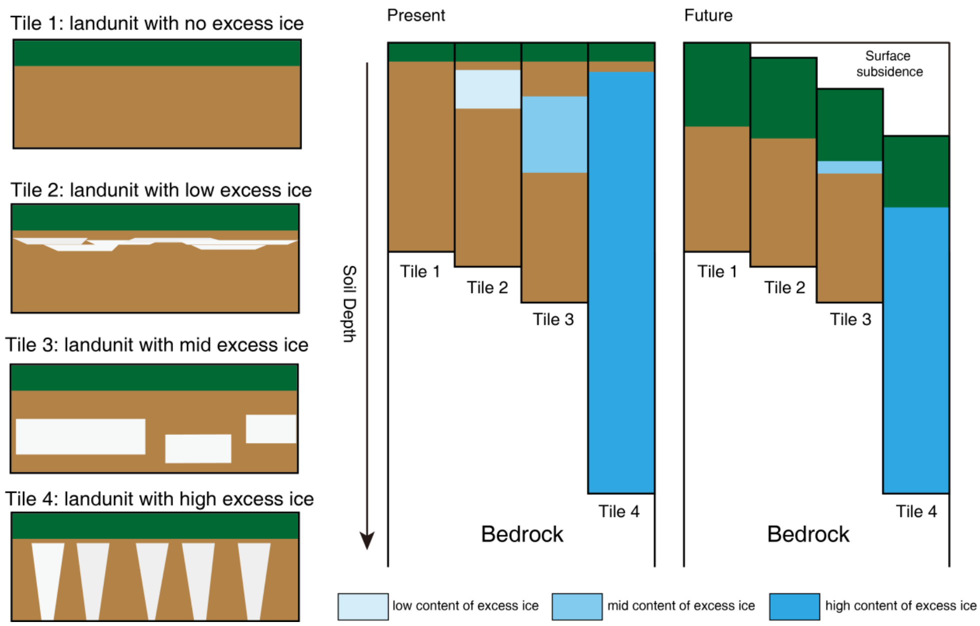

Figure 4. A schematic representation of the excess ice initialization scenario in the global simulation case 4 and how the excess ice potentially melts in the future.

https://doi.org/10.5194/tc-2019-230
Preprint. Discussion started: 7 October 2019

The Cryosphere
Discussions
Open Access

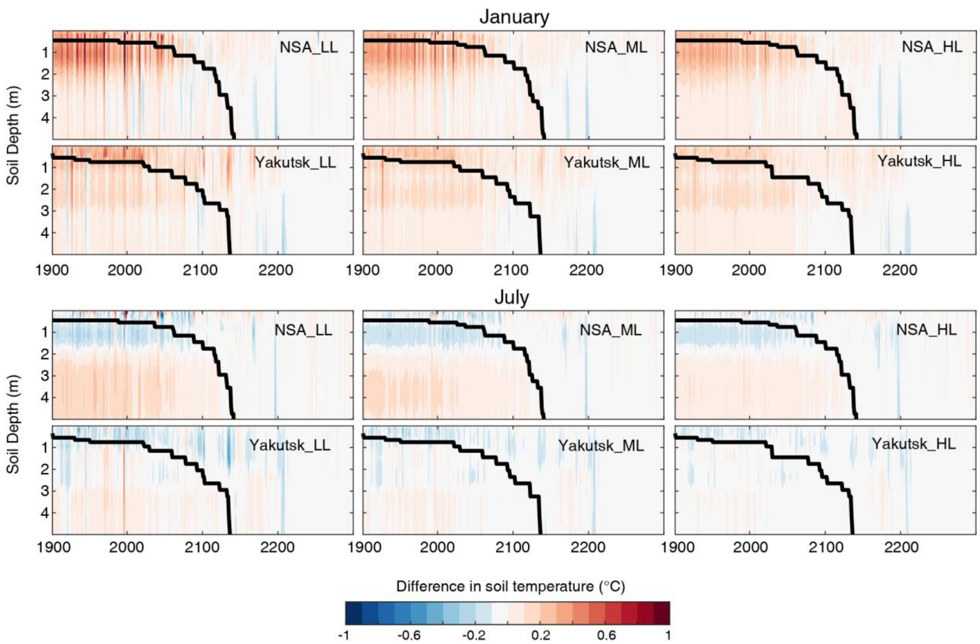

535 **Figure 5: Soil temperature differences from excess ice cases to control cases (NSA_control and Yakutsk_control) for the depth of 0.005-5 meters in January and July. Black lines are the active layer depth deepening through time. The active layer depth is calculated from grid-scale soil temperature for each case.**

https://doi.org/10.5194/tc-2019-230
Preprint. Discussion started: 7 October 2019

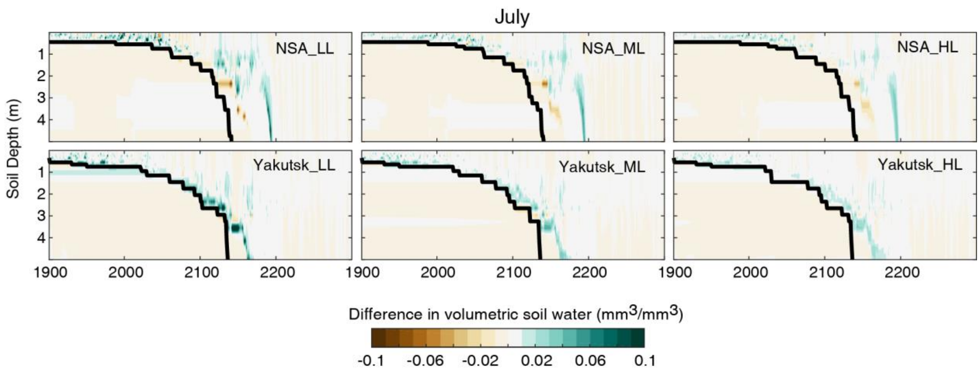

540 **Figure 6: Soil moisture differences from excess ice cases to the corresponding control cases (NSA_control and Yakutsk_control) for the depth of 0.05-5 meters in July. Black lines are the active layer depth deepening through time. The active layer depth is calculated from grid-scale soil temperature for each case.**

545

https://doi.org/10.5194/tc-2019-230
Preprint. Discussion started: 7 October 2019

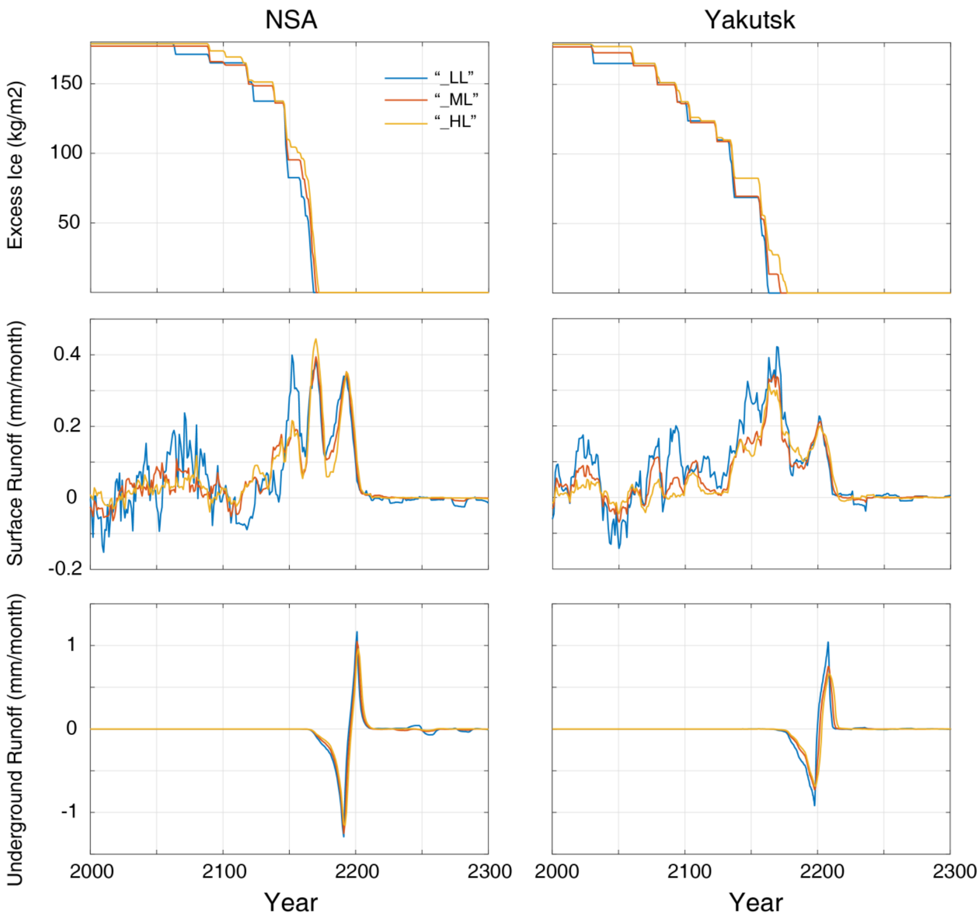

Figure 7: Time series of excess ice (kg/m^2), as well as the difference of surface runoff (mm/month) and subsurface drainage (mm/month) from the three excess ice cases to control cases. A 15-year moving average is applied before plotting both the surface and underground runoff.

550

https://doi.org/10.5194/tc-2019-230
Preprint. Discussion started: 7 October 2019

The Cryosphere Discussions
Open Access
EGU

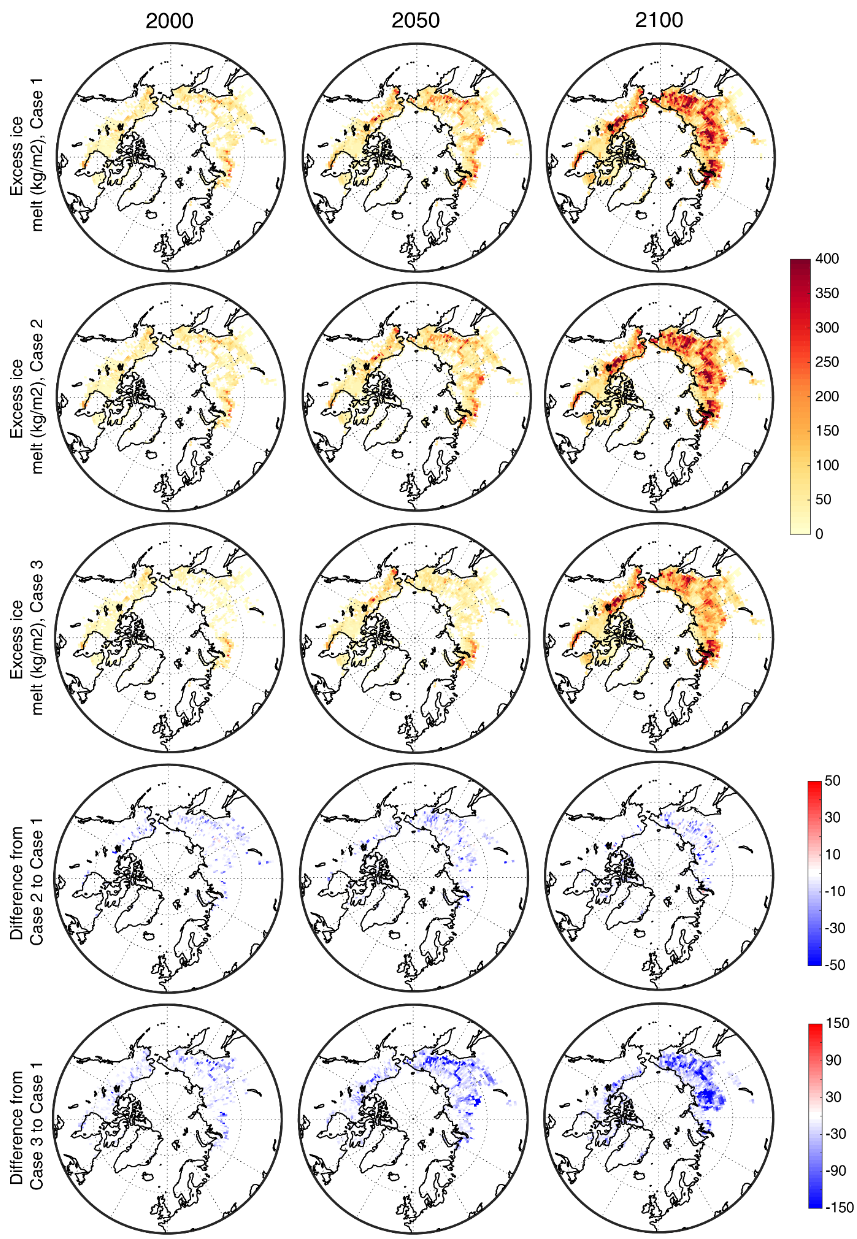

Figure 8 The global distribution of excess ice melt (kg/m^2) at 2000, 2050, and 2100 in case 1 to 3, as well as the differences of excess ice melt compared to that in case 1.

555

https://doi.org/10.5194/tc-2019-230
Preprint. Discussion started: 7 October 2019

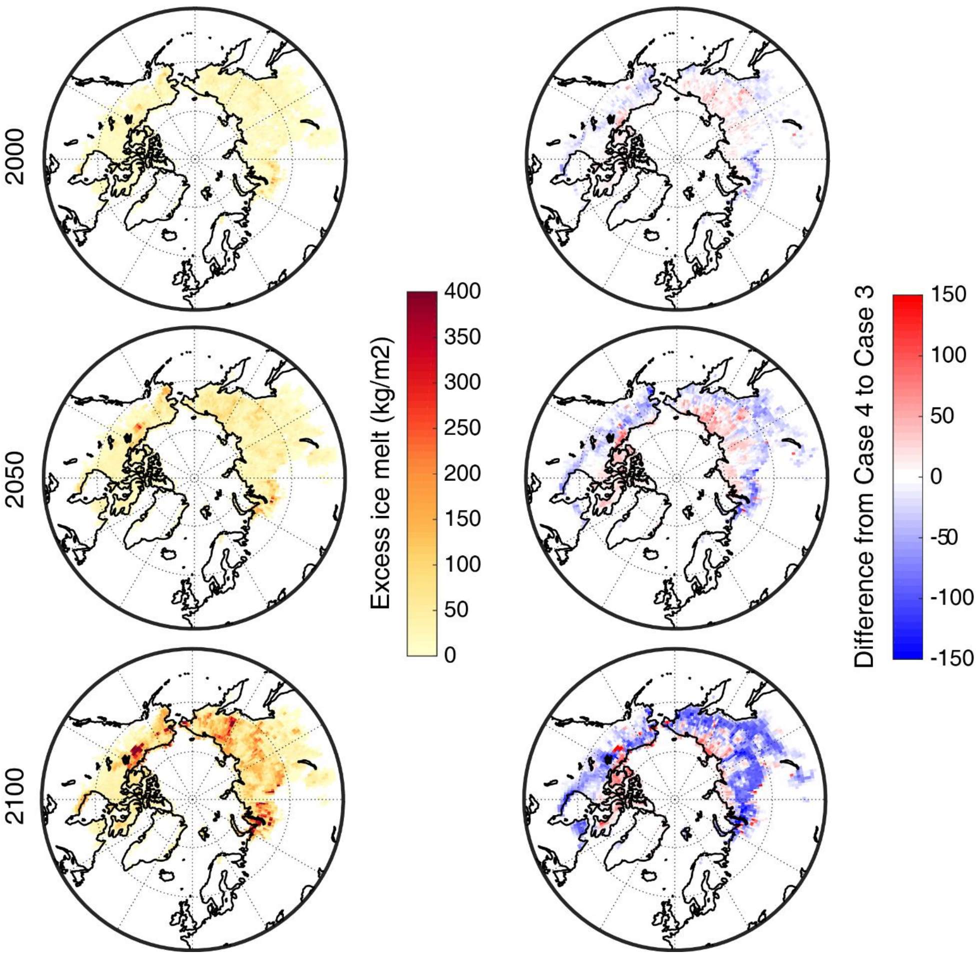

Figure 9: The global distribution of excess ice melt (kg/m^2) at 2000, 2050, and 2100 in case 4 (left), as well as the differences of excess ice melt between case 4 and case 3 (right).

560

https://doi.org/10.5194/tc-2019-230
Preprint. Discussion started: 7 October 2019

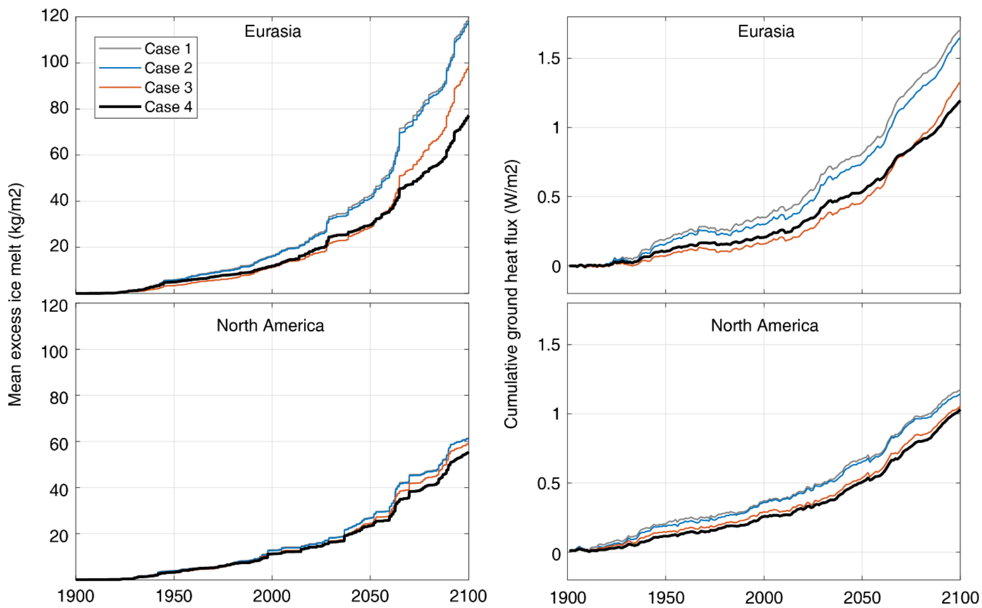

Figure 10: The excess ice melt (kg/m^2) and cumulative ground heat flux (W/m^2) averaged for all grid points with excess ice initialized in two Arctic regions of Eurasia (60-80 N, 60-180 E) and North America (60-80 N, 60-180 W).

565